ARTICLES
https://doi.org/10.1038/s41563-020-0699-3
nature materials

Resilient yet entirely degradable gelatin-based biogels for soft robots and electronics

Melanie Baumgartner[1,2,3,7], Florian Hartmann[1,2,7], Michael Drack[1,2], David Preninger[1,2], Daniela Wirthl[1,2], Robert Gerstmayr[2,3], Lukas Lehner[1,2], Guoyong Mao[1,2], Roland Pruckner[1,2], Stepan Demchyshyn[1,2], Lisa Reiter[1,2], Moritz Strobel[3], Thomas Stockinger[1,2], David Schiller[1,2], Susanne Kimeswenger[1,2,4], Florian Greibich[1,2], Gerda Buchberger[5,6], Elke Bradt[3], Sabine Hild[3], Siegfried Bauer[1,8] and Martin Kaltenbrunner[1,2] ✉

Biodegradable and biocompatible elastic materials for soft robotics, tissue engineering or stretchable electronics with good mechanical properties, tunability, modifiability or healing properties drive technological advance, and yet they are not durable under ambient conditions and do not combine all the attributes in a single platform. We have developed a versatile gelatin-based biogel, which is highly resilient with outstanding elastic characteristics, yet degrades fully when disposed. It self-adheres, is rapidly healable and derived entirely from natural and food-safe constituents. We merge all the favourable attributes in one material that is easy to reproduce and scalable, and has a low-cost production under ambient conditions. This biogel is a step towards durable, life-like soft robotic and electronic systems that are sustainable and closely mimic their natural antetypes.

In 2025, an estimated six million tons of garbage will be generated per day[1], with tech disposables being a rapidly growing contributor. End-of-lifetime appliances contain valuable materials that are laborious to recover or toxic substances that are readily released into nature through landfilling or improper treatment[2]. Biodegradable[3–6] and transient systems[7] are promising routes towards closing the loop on waste generation and create new opportunities for secure systems, but often at the cost of compromises in performance. Complex biological systems bridge this gap. They unite seemingly antagonistic properties—tough yet adaptive, durable and self-healing yet degradable—which allows them to perform a myriad of intricate tasks. Embodiments of technologies that intimately interface with humans naturally benefit from mimicking such soft, functional forms. A range of biomimetic systems[8], which include soft machines[9] and electronic skins (e-skins)[10], achieve a high level of functionality by introducing self-healing[11,12], intrinsic stretchability[13] or the insightful merging of soft-to-hard materials[14]. Waste flow issues and in vivo applications that avoid multiple surgeries are tackled with inextensible devices in the form of edible[3,15] and transient electronics[7,16]. However, introducing stretchability to degradable devices remains challenging. Recent approaches that focus on stretchable biodegradable sensors[5] require expensive materials and are still wired to bulky measurement systems, which hinders their implementation as wearable devices. Challenges here stem from the diverse material requirements, which range from mechanical resilience, durability and stretchability to high processability and low cost, and yet be entirely degradable. Synthetic materials, such as polyester-based elastomers[17–20] or polyurethanes[21], degrade slowly and necessitate time- and energy-consuming synthesis, which may hamper their widespread market introduction. Bioderived hydrogels[22–24] based on starch, alginate or collagen are cheap and offer fast degradation rates, but typically fail to provide a sufficient mechanical integrity under high loads. Strategies based on photocrosslinking[25], the inclusion of additional monomers[26,27] or salt treatment[28,29] help to overcome this issue, but at the cost of processability, degradability and price (Table 1).

Gelatin-based gels are a promising choice, as such biopolymers are readily derived without the need for synthesis, allow for water-soluble additives, are harmless to the environment due to fast degradation rates and are even edible. Known to humankind for millennia, gelatin evolved from naturally derived glue to a widely used material in photographic films, food production, cosmetics and medications[30]. Applications of gelatin now span a diverse field from drug delivery[31] and bone-tissue engineering[32], which includes three-dimensional (3D) printed scaffolds[33] and (micro)robotics[34] operated in vivo. Yet, so far, gelatin-based gels have a moderate performance when strained and rapidly dry when operated in air, which causes stiffening and limits the stability and durability of wearable soft devices or soft robotic elements (Table 1 and Supplementary Tables 1 and 2). Existing examples of gelatin-based biodegradable soft actuators partially address these issues by maintaining a certain level of stretchability in the dried state[24], operating in salt-gradient electrolyte solutions[35] or using off-the-shelf confectionary gels[36]. However, all suffer from difficult-to-control material properties and limited stretchability which leads to a reduced performance of a few actuation cycles only.

Here we introduce a fabrication approach, design rules and a set of concepts for a broadly applicable gelatin-based biogel that unites the challenging needs of resilient yet sustainable (soft) robots and electronics in a single platform. Our gel is based on naturally

[1]Division of Soft Matter Physics, Institute for Experimental Physics, Johannes Kepler University Linz, Linz, Austria. [2]Soft Materials Lab, Linz Institute of Technology, Johannes Kepler University Linz, Linz, Austria. [3]Institute of Polymer Science, Johannes Kepler University Linz, Linz, Austria. [4]Department of Dermatology and Venerology, Kepler University Hospital, Linz, Austria. [5]Institute of Biomedical Mechatronics, Johannes Kepler University Linz, Linz, Austria. [6]Present address: Institute of Applied Physics, Johannes Kepler University Linz, Linz, Austria. [7]These authors contributed equally: Melanie Baumgartner, Florian Hartmann. [8]Deceased: S. Bauer. ✉e-mail: martin.kaltenbrunner@jku.at

Table 1 | Materials selection matrix for biodegradable elastomers

		Shelf life	Mechanics	Cost	Processability	Synthesis	Degradation
Polyesters	POC[17,18]	NA	+	€€€	●●	+	>6 m
	PGS[19]	NA	+	€€	●●	+	several weeks
	PCL -co-PLA[20]	15 d	-	€€€	●●●	+	6 to >24 m
	Polyurethanes[21]	NA	+	€€€€€	●●●	+	6 to >24 m
Hydrogels	PLS[22]	<30 d	-	€€	●●●	-	<10 d
	Starch/silicone[27]	NA	+	€€	●●	-	3–6 yr
	HA hydrogel[23]	NA	-	€€€	●	-	2 m
	Gelatin/glycerol[24]	NA	-	€	●●	-	<10 d
	Gelatin/salt treated[28]	NA	+	€	●●	-	<10 d
	GelMa[25]	<6 m	-	€	●	+	<10 d
	PVDT-GelMa[26]	NA	+	€€€€	●	+	<10 d
	Gelatin biogel (this work)	>13 m	+	€	●●●	-	<10 d

Selection of biodegradable elastomers and hydrogels that are possible candidates for soft robotics and electronics[17–28]. An expanded version and selection criteria are given in the Supplementary Information. POC, poly(1,8-octanediol citrate); PGS, poly(glycerol sebacate); PCL, poly(ε-caprolactone); PLA, poly(lactic acid); HA, hyaluronic acid; PLS, plasticized starch; GelMa, methacrylated gelatin; PVDT, poly(2-vinyl-4,6-diamino-1,3,5-triazine); NA, not available.

occurring materials as degradable building blocks that are durable, self-adhering, stretchable, mechanically tunable and healable. Despite being entirely degradable when disposed in wastewater, our gels maintain their mechanical properties for more than one year under ambient conditions and enable soft actuators that operate for more than 330,000 cycles without failure. Scalable production, low material costs and safety of all the fabrication steps will enable a widespread employment, from industry and healthcare to education. Inspired by sophisticated living beings, from cephalopods to elephants, we combined our biogel with naturally derived materials, such as cellulose and zinc, to achieve fully biodegradable devices from robotic elements to stretchable electronics.

Cellulose as a prevalent structural polysaccharide serves as a textile exoskeleton for soft pneumatic biogel actuators (Fig. 1a) designed to operate in dynamic environments. Combining the biogel with structured zinc electrodes allows fully degradable sensor skins (Fig. 1b), which paves the way for future biomedical devices that mimic our own skin. Our mechanically resilient biogel is an ideal material for temporary installations or frequently renewed applications that profit from transient devices as it breaks down into its building blocks within a few days (Fig. 1c and Supplementary Videos 1 and 2) if triggered. The biogels are cleaved enzymatically by wastewater bacteria within five days, which renders the biogel readily biodegradable according to the standards of the Organisation for Economic Co-operation and Development (Fig. 1d, Extended Data Fig. 1 and Supplementary Methods). Unlike simple dissolution that does not alleviate environmental concerns and may ultimately hamper in vivo applications through accumulation in filtration systems, such as the kidney[37], the more complete chemical degradation of individual polymer chains of gelatin enables disposal by the body and fully sustainable devices[38]. Where required, the dissolution onset of our biogels is substantially delayed in aqueous media and even in simulated stomach fluids using hydrophobic biodegradable coating strategies based on shellac resins (Methods and Supplementary Video 3). Coated biogels show no signs of dissolution after 48 h of immersion in water or 24 h in acidic solution (pH 2.1). The degradation of the encapsulation layer is triggered in basic solutions (here pH 8.1), followed by the complete dissolution of our biogel. This may open up routes for biodegradable applications in water or in vivo.

We combined a variety of components—each serving a distinct purpose—to benefit from both biodegradation and a high mechanical performance at the same time. Gelatin as the main polymer network of the gel defined the material's Young's modulus (E) and the addition of sugars boosted extensibility. Stable mechanical properties and processing conditions were achieved by tuning the ratio of water and glycerol within the biogel, and citric acid prevented bacterial growth. Food-grade additives introduced additional functionalities or structural properties without compromising the eco-friendliness and safety of the material (Supplementary Fig. 1). Detailed design rules that yield resilient and tough gels and compositions are given in the Supplementary Discussion and Supplementary Table 3.

The wide range of emerging soft electromechanical systems—from e-skins to robotics—demands a set of reliable and durable materials with readily tunable mechanical properties. We adjusted E and the ultimate (engineering) stress (σ_u) of our biogel by an order of magnitude (~30 to ~300 kPa and ~10 to ~140 kPa, respectively) by modifying the amount of gelatin, both of which scale nearly exponentially with gelatin concentration (Fig. 2a and Supplementary Fig. 2a). Concurrently, the ultimate strain (ε_u) increased from a 180 to 325% linear strain (Fig. 2b). Higher values of E (3.1 MPa) were achieved by further increasing the gelatin concentration (Supplementary Fig. 2b), with improvements of σ_u (1.86 MPa), but a somewhat reduced ε_u (254%). The high extensibility of our biogels was enabled by adding 28 wt% sugar syrup, which increased both σ_u and ε_u (Fig. 2c,d and Supplementary Fig. 3a). The addition of sugars (and glycerol) as co-solvents drives biopolymer–biopolymer (helix–helix) association, enhances gelation and thermodynamically stabilizes gelatin gels[39], with an overall favourable impact on the network formation. We hypothesized that unzipping these helix–helix associations under high deformations leads to the observed increased extensibility. As a variety of food-safe additives interact with the gelatin network, we achieved outstanding properties through meticulous and systematic optimization of all the constituting materials.

Despite its high stretchability, our biogel showed a small hysteresis on repeated cyclic, which stretched to a 100% linear strain with a constant energy dissipation after the second cycle of 6.4 kJ m^{-3} (Supplementary Fig. 4a,b). Limited fatigue set in after thousands of stretch–release cycles, yet no failure occurred after more than 100,000 cycles (Supplementary Fig. 5). Modifying the concentration of the base biopolymer provided a frugal route towards tuning the mechanical properties; likewise, it influenced gelation, thermal stability and processability. Gelling time decreased from 12 to 5 min,

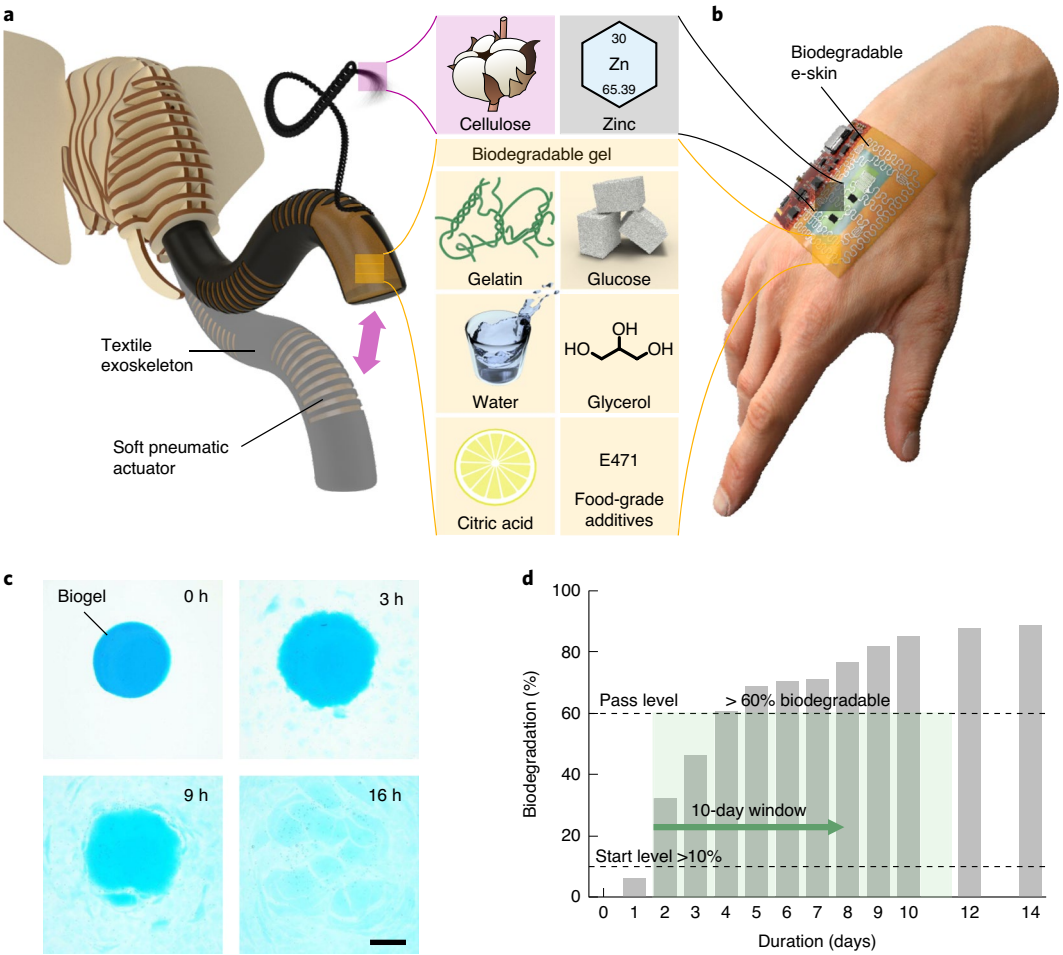

Fig. 1 | A resilient yet fully degradable biogel. a,**b**, Naturally derived ingredients, such as gelatin and citric acid, enable an elastic and stable, but fully degradable, biogel. Together with cellulose fibres and zinc, soft and durable pneumatic actuators (**a**) and multifunctional e-skins (**b**) are realized. **c**, A food-coloured biogel disc immersed in deionized water at 23 °C dissolves within several hours. Scale bar, 1 cm. **d**, Complete aerobic decomposition of the biogel, measured via biological oxygen demand (BOD) of the microorganisms in the test solution (wastewater). The pass level for ready biodegradability is the removal of 60% of dissolved organic compounds in a 10-day window.

whereas gelling temperature increased from 39 to 50 °C by doubling the amount of gelatin, which expanded its operational temperature range (Supplementary Fig. 6). Gelatin concentrations above 50% complicated the manual fabrication, but potentially provide stiffer material solutions in combination with advanced fabrication techniques, such as injection moulding or 3D printing.

Overcoming the drawback of water-rich polymers—hydrogels suffer from dehydration when used in ambient conditions owing to a loss of free water—we replaced large water fractions with the non-volatile food additive glycerol (a softener and humectant) to reduce the amount of free water in our biogels. A decreasing water–glycerol ratio extends the storage time and stability without influencing the mechanical properties. Consequently, the dehydration-related weight loss of the biogel was reduced from 25% (G1620 formulation) to <5% (G1644 formulation) when stored in ambient conditions for ~100 h (Fig. 2e) and remains below 10% even in a very dry environment (23 °C and 20% relative humidity (RH); Supplementary Fig. 7). Additionally, increasing the glycerol concentration (from 20 to 36 wt%) cancelled unwanted material stiffening (Fig. 2f) and led to nearly constant mechanical properties within 392 days of storage time in ambient air (Fig. 2g). These modifications enabled a reliable stress–strain behaviour and the fabrication of form-stable devices (Fig. 2h). No signs of material degradation were observed over the course of one year. We note that these experiments were stopped due to time constraints only, which suggests that our biogels are stable for even longer time periods. Reducing the pH value of our biogels by the addition of citric acid prevented bacterial growth but did not influence its stretchability (Fig. 2i and Supplementary Figs. 3b and 8). Electing the constituent concentrations allowed us to design a deformable and elastic biogel that does not dry out and is suitable for soft robotic applications operable within humidity ranges of 20–80% RH (Supplementary Figs. 7 and 9). Biaxial stretching tests, performed by inflating a biogel disc into a balloon shape (Fig. 2j, Supplementary Fig. 10 and Supplementary Video 4), confirmed areal strains beyond 1,000%. We modelled the strain distribution throughout the inflated balloon with a finite element method (FEM), which showed a linear strain of 242% at its apex (Fig. 2k), equivalent to an over 1,000% areal strain (Fig. 2l). Even with a notch in the sample, the biogel withstood 109 J m^{-2} before crack propagation (Supplementary Fig. 11). Introducing biodegradable co-networks that potentially boost the gels fracture toughness may, in future, allow extremely soft yet tough biogels.

So far, soft robotic[40] and (wearable) healthcare applications[41] almost exclusively employ silicones or polyurethanes, which are barely degradable. Although reliable high-performance materials are often a necessity, many tools from electrocardiography electrodes to wound patches or endoscopy tubes are single-use devices,

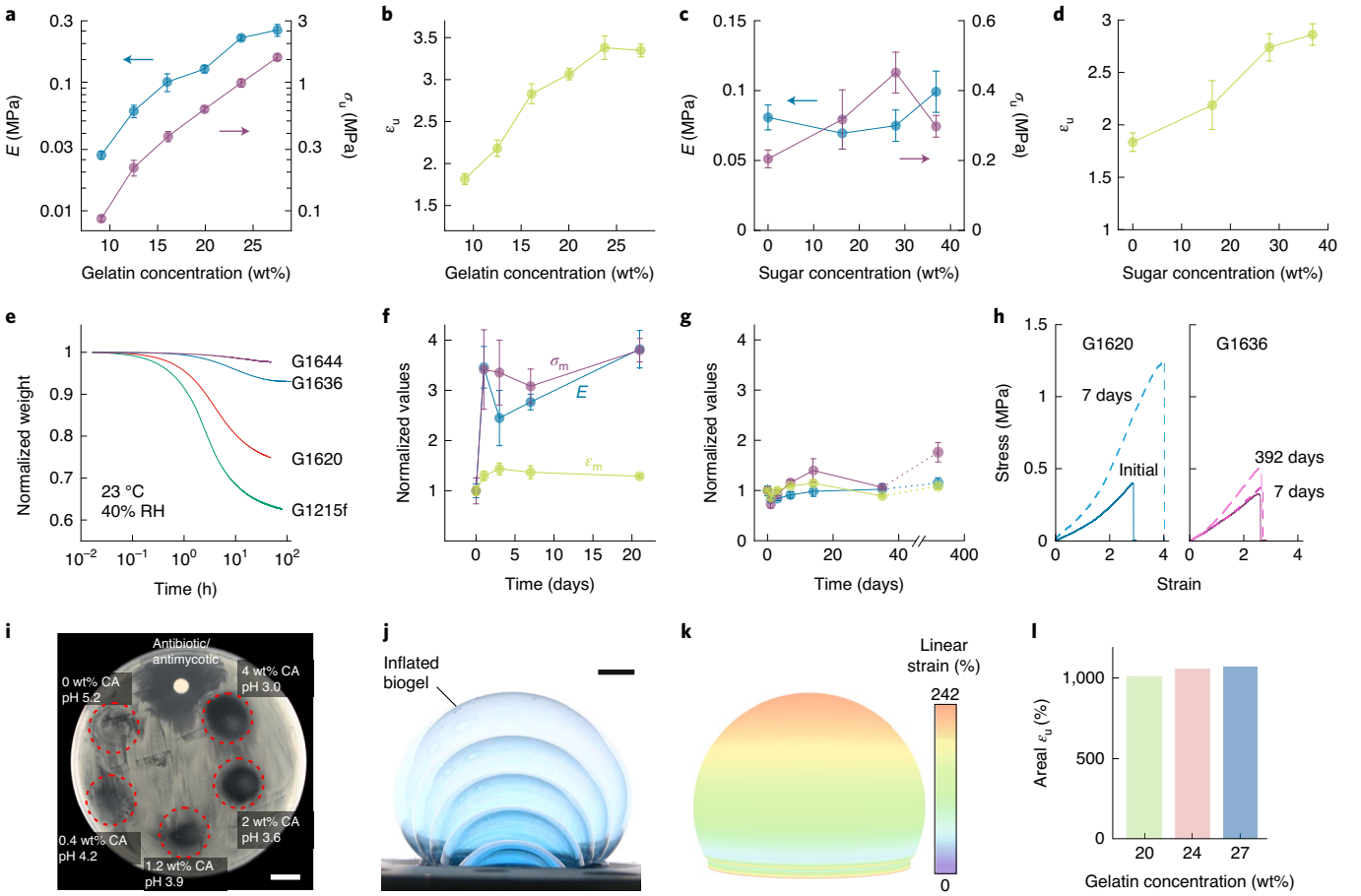

Fig. 2 | Tunability, stability and extreme mechanics of gelatin biogels. a, E (blue line) and σ_u (purple line) increased strongly with higher gelatin concentrations. **b**, ε_u of the dumbbell-shaped samples increased substantially for gelatin concentrations up to 25 wt% and reached saturation for higher values. **c**, E and σ_u as a function of sugar concentration. Although E changed only slightly, σ_u maximized at 28 wt%. **d**, ε_u increased with sugar concentration, with only small changes above 28 wt%. **e**, The dehydration process of freshly prepared biogel samples of different water concentrations. **f**, Evolution of E (blue line), σ_u (purple line) and ε_u (green line) of a water-rich gel formulation (G1620). Within one day, E and σ_u increased by a factor of three, whereas ε_u stayed unaffected. **g**, E (blue line), σ_u (purple line) and ε_u (green line) of a low-moisture gel formulation (G1636) showed no substantial age-related changes when stored in ambient conditions for more than one year (392 days). **h**, Replacing parts of the water fraction with glycerol showed a minor influence on the stress–strain behaviour that otherwise quickly changed for water-rich compositions. **i**, Increasing the citric acid (CA) concentration prevented bacterial growth. Scale bar, 1 cm. **j**, Balloon-type inflation of a biogel membrane (G2820) in several actuation states. Scale bar, 1 cm. **k**, Mechanical simulation of an inflated biogel balloon. The maximum linear strain (longitudinal direction) was located at the apex of the balloon. **l**, Ultimate areal strain during balloon inflation of gels with varying gelatin concentration. G1620, green; G2420, red; G2820, blue). **a**–**d**, Error bars: s.d. for $n > 5$ measurements. **f**,**g**, Error bars: s.d. for $n > 4$ measurements.

operated for a short time. In addition, inherently safe and even edible elastic gels open up a cornucopia of applications from toys for children to robots that imitate other animals for behaviour studies or prey imitation[42].

Our biogel uniquely combines high performance and degradability, which renders it suitable for soft (bio)robotics, medical appliances and industrial robotic grippers disposed of after their application. We here demonstrate the potential with a soft pneumatic actuator inspired by an elephant's trunk. The s-shaped movement of the pneumatically driven actuator reaches 10-cm-maximum displacement of its tip (Fig. 3a). The actuator consists of a cast biogel tube with a flexible air inlet and a textile exoskeleton made from crocheted cotton fibres, which direct the movement (Fig. 3b and Supplementary Figs. 12 and 13). We chose two pattern designs that result in s-shaped and u-shaped (simple bending) motion (Supplementary Fig. 14 and Supplementary Video 5), which imitate the lift and grab movements of a trunk. The number of actuation cycles was monitored by inflating the u-shaped actuator with a constant pressure against a plate connected to a force sensor. Actuators made from a high water/glycerol ratio biogel (G2420) endured up to 10,000 cycles (~10 h of constant actuation) and are promising for applications for which an intermediate durability is sufficient, such as customized rehabilitation actuators or rescue robots that operate in hazardous environments. Actuators with a lower water/glycerol ratio (G2430) are highly durable and showed no failure even after 60,000 cycles. Here, the actuation force dropped to 40% of the original value during the course of the experiments (two days) due to some material fatigue (Supplementary Fig. 15). Using a force-regulated set-up (adjusting the actuation pressure and frequency) boosted cycle lifetime to more than 330,000 cycles without failure (Fig. 3c and Supplementary Fig. 16), which outperforms existing approaches by four orders of magnitude[24,36] and enables the integration of actuators or grippers in fabrication lines or as harvesting robots for otherwise hand-picked produce[8,43,44]. Actuators operated for over 1.5 h and ~2,000 cycles, even underwater when coated with edible oil (Supplementary Video 6). By constraining the

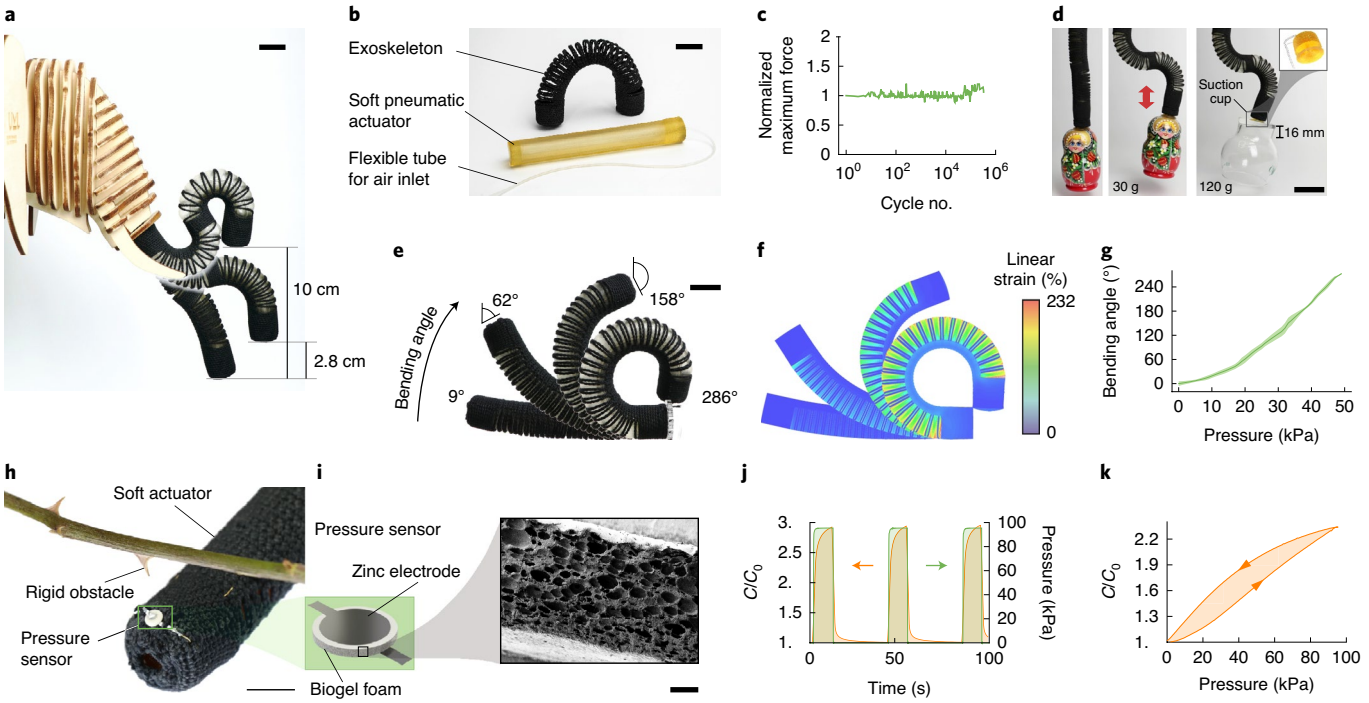

Fig. 3 | Resilient biogels for soft actuators. a, Flexure of an s-shaped tube actuator. The fully deflected trunk achieves a displacement of 10 cm in the vertical direction. Scale bar, 2 cm. **b**, Textile exoskeleton and inner gel tube of a soft pneumatic actuator. Scale bar, 2 cm. **c**, Cyclic actuation of a u-shaped actuator in ambient conditions. The actuator achieved over 330,000 cycles without failure in a force-regulated set-up, using a low-moisture gel composition (G2430). **d**, A gel suction cup attached to the actuator (actuator weight ~35 g) allowed the lifting of variously shaped objects with a weight of up to 120 g. Scale bar, 4 cm. **e**, Several states of a u-shaped bending actuator. At the maximum angle, bending is blocked by self-collision. Scale bar, 2 cm. **f**, Mechanical simulation of the u-shaped bending actuator. The linear strain is along the longitudinal direction of the actuator. **g**, The correlation between the bending angle and applied pressure follows a linear behaviour between 60° and the maximum angle. The mean (solid line) and s.d. (shaded area) for four consecutive measurements. **h**, A biodegradable pressure sensor on a u-shaped actuator provided feedback from potential dangers, such as a rose thorn. Scale bar, 1 cm. **i**, Scanning electron microscopy (SEM) image of the biogel foam cross-section. Scale bar, 200 µm. **j**, Pressure profile and responding capacity change (C) of a pressure sensor. C_0, capacity measurement at the start. **k**, The characteristic for the pressure sensor shows a small hysteresis.

movement of the tip, we showed that they achieve a maximum force of 14.7 N at an applied pressure of 102 kPa (Supplementary Fig. 17).

Adding a biogel suction cup to the tube (connected to a vacuum pump) enabled the grasping and lifting of diverse objects with flat or curved shapes up to 120 g for a distance of 16 mm (Fig. 3d and Supplementary Video 7). The u-shaped design enabled bending angles of up to 286° (Fig. 3e), which correspond to a maximum linear strain of 232%, calculated from modelling the strain distribution of the actuator with FEM (Fig. 3f). The full-range bending angle of 281° was achieved by applying a pressure of 50 kPa (Fig. 3g). Discrete positions are reliably adjusted with an automated pressure-control system (Supplementary Fig. 18). Additional functionalities, such as faunal defence mechanisms, were directly incorporated by adding fluorescent dyes. Such modified actuators glow in the dark under ultraviolet illumination, which indicates the actuated state, whereas the relaxed state appears dark due to the covering textile (Supplementary Fig. 19 and Supplementary Video 5). The exoskeleton of our biogel actuator provided a platform that was easily manufactured with tools as simple as crocheting hooks and allowed the fast prototyping of our safe kids-toy robot, 'Percy the Gellyfant' (Extended Data Fig. 2 and Supplementary Video 8). Yet, it can readily be enhanced with biodegradable sensors to provide improved feedback and control. A biodegradable capacitive pressure sensor added a tactile sense to our actuator and helped to recognize obstacles. We utilized the food additive mono- and diglycerides of fatty acids (E471) to create stable air bubbles within the biogel volume. Sandwiched between two zinc electrodes, this foam acted as a deformable capacitor (Fig. 3h and Supplementary Video 9) which enabled the actuator to react to obstacles, such as a rose thorn. Applying a load compressed the voids in the soft foam (Fig. 3i) and approached the two electrodes, which resulted in an impedance change. We achieved a capacity change of a factor of three at repeated compressions with a 100 kPa load (Fig. 3j). The slight hysteresis resulted from the foams mechanical response (Fig. 3k and Supplementary Fig. 4c,d), which exhibited a larger energy dissipation compared with that of the incompressible biogel (G1620) due to the enclosed air voids.

Soft robots equipped with multimodal sensing capabilities provide the necessary environmental feedback and will bring them a step closer to autonomy. One possible route to further improve robots is to implement soft e-skins[45] to provide information about temperature, humidity or the state of deformation. The seamless integration of such e-skins on soft bodies is beneficial for robots and humans alike, and may enhance wearable appliances from consumer electronics to medical diagnostic tools. However, the high throughput of medical appliances and their stringent hygiene requirements decrease their operational lifetime, which raises demand on biodegradable solutions. Our biogel presents a self-adhering platform for biodegradable soft electronics that adheres to various surfaces without additional adhesives. We demonstrate autonomous sensor patches that are rapidly assembled from our tunable biogels by taking advantage of their thermoplastic properties.

Healing or assembly of the biogel was accomplished by a brief local melting near a crack or cut with an infrared laser (Fig. 4a). Laser

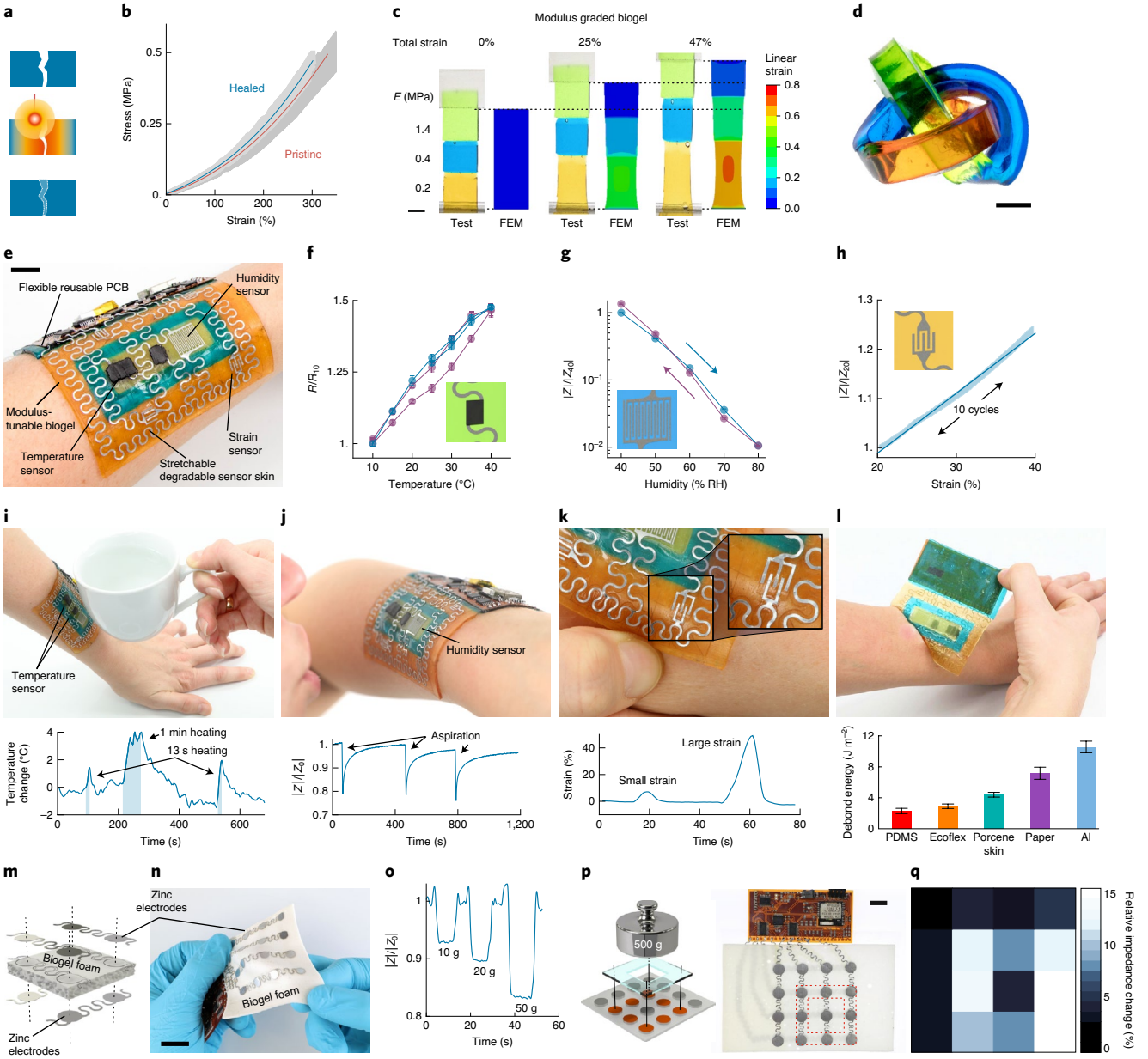

Fig. 4 | Soft and degradable electronic sensor patches. a, Schematic of the LARH process. Edges to be joined were brought into near contact and selectively heated by a laser beam. A local liquefaction process allowed a seamless bond. **b**, Stress–strain measurements of pristine and cut-and-healed gel samples (G1620) showed no decrease in mechanical properties. The polynomial fit (solid lines) and data envelope (grey shadows) are for seven individual samples each. **c**, Tensile test of a modulus-graded gel compared with its FEM simulation. The strain was along the stretching direction. Scale bar, 1 cm. **d**, A trefoil knot of three different gels (G1730, G2430 and G3030) assembled by LARH. Scale bar, 5 mm. **e**, Soft e-skin on a human arm. Scale bar, 3 cm. **f**, Characteristics of the biodegradable temperature sensor (inset). The signal shows hysteresis during the third (purple) cycle, but it vanishes after the fourth (blue). Error bars, s.d. for a measurement period >10 min. R, resistance; R_{10}, resistance at 10 ºC. **g**, Characteristics of a humidity sensor (inset). Error bars, s.d. for a measurement period >10 min. Z, impedance; Z_{40}, impedance at 40% RH. **h**, Performance of the strain sensor (inset). The regression over ten cycles demonstrated a linear response. Linear fit (solid line) and data envelope (blue shade) for ten consecutive strain cycles. Z_{20}, impedance at 20% RH **i**, An on-skin-worn electronic patch was exposed to elevated temperatures (top). Exposures of different durations were recorded (bottom). **j**, Repeated aspiration onto the electronic patch (top) and resulting peaks in the humidity recordings (bottom). Z_0, impedance at the start. **k**, Mechanical deformation of strain sensors (top) and recordings for two different strain levels (bottom). **l**, Peel-off of the electronic patch (top). The debond energy was measured for G1644 on different substrates (bottom). Scale bar, 3 cm. Error bars, s.d. for n > 3 measurements. **m**, Schematic showing orientation and design of zinc electrodes on biogel foam G1215f. **n**, Degradable stretchable pressure sensor array. Scale bar, 2 cm. **o**, Impedance response of a single pressure sensor impinged by different weights. **p**, Schematic and photograph of a 500 g weight distributed to a square shaped part of a 4 × 4 pressure sensor array. Scale bar, 1 cm. **q**, Signals recorded with the pressure-sensor patch. PDMS, polydimethylsiloxane.

healing of previously dissected biogels essentially fully restored their original mechanical properties (Fig. 4b) within less than 10 min of the process time. We used this laser-assisted rapid healing (LARH) to assemble biogels with different E values (1.4, 0.4 and 0.2 MPa) into graded modulus gels. Uniaxial stretching of such modulus-graded biogels reduced the strain in the stiffest part by 90% at an overall

strain of 50% (Fig. 4c). We modelled the strain distribution by FEM and analytical calculations, and found good agreement with experiments in both cases (Supplementary Fig. 20). Rapid assembly with LARH allowed us to realize complex 3D shapes, such as a trefoil knot (Fig. 4d), or tailored, sophisticated substrates for stretchable electronics. We manufactured a biodegradable, stretchable multimodal e-skin, which had temperature, humidity and strain sensors, using our biogel (Fig. 4e, Extended Data Fig. 3 and Supplementary Fig. 21, Supplementary Fig. 22). The sensors, structured from zinc foil or temperature-sensitive paste, were addressed by zinc meanders stretchable to a 50% uniaxial strain without a change in resistance as they endured more than 1,000 cycles when stretched to 20% (Extended Data Fig. 4a–c). The sensor data was recorded, analysed and transmitted wirelessly by utilizing a reusable flexible printed circuit board (PCB) unit mounted on the biogel. This PCB featured multichannel-impedance recording, analogue–digital converters, current sources and Bluetooth communication on a single autonomous platform (Supplementary Figs. 21 and 23). We chose this cost-effective approach as the PCB is readily recycled and, so far, broadband wireless data communication, such as Bluetooth, is still elusive in degradable form factors. Future research will focus on overcoming this bottleneck by implementing basic functionality using transient radio-frequency transistor technology.

The temperature sensor made from a mixture of carnauba wax and graphite powder shows a nearly linear resistance response in a temperature range from 10 to 40 °C (Fig. 4f and Extended Data Fig. 4g,h). The humidity sensor, designed as an interdigital electrode, followed an exponential decrease in impedance with increasing RH (Fig. 4g). The change in impedance spanned more than two orders of magnitude, yet its response to mechanical deformation was negligible due to its strain-isolated design (Extended Data Fig. 4d–f). The high number of fingers in combination with the graded modulus biogel greatly reduced the strain on the humidity sensor. Reducing the number of fingers and increasing their spacing allowed a large displacement of the electrodes on a soft biogel and rendered a strain sensor with a linear response, but showed no hysteresis under cyclic stretch (Fig. 4h and Extended Data Fig. 4i,j). The sensor skin monitored temperature variations in proximity to a hot cup (Fig. 4i), humidity changes induced by aspiration (Fig. 4j) or deformation of the skin (Fig. 4k). The intrinsically adhesive biogel adhered to various surfaces, as evidenced with 90° peel tests (Fig. 4l and Extended Data Fig. 5). In particular, we showed a stable interfacing with human skin even under twisting or shaking, but in addition allowed for the removal of the sensor patch without skin irritation (Supplementary Video 10). The biogel adhered to human skin even under elevated movement during sports and while sweating (Extended Data Fig. 6a–f). No signs of skin irritation were visible after 7 h of wear. Prolonged contact with the skin did not alter the mechanical properties of our biogels, which remained constant even after 38 h of cumulative wear time during 4 days of routine daily activities (Extended Data Fig. 6g–j). Non-sticky versions were achievable if covered with talcum powder (Supplementary Video 11). Highly stretchable films with submillimetre thicknesses were readily fabricated using doctor blading (Supplementary Video 12). Based on our concept of a capacitive biodegradable pressure sensor, we designed a pressure-sensitive e-skin array from a 1-mm-thick biogel foam together with a 4×4 matrix of zinc-foil electrodes with stretchable interconnects (Fig. 4m,n). The stretchable pressure sensor array was addressed and read out by the flexible PCB (Fig. 4o, Extended Data Fig. 7 and Supplementary Video 13). Besides being able to quantify a load on a single specific sensor, the pressure sensor array detected objects with complex shapes (Fig. 4p,q). When stored in ambient conditions, our e-skins remained functional for over a year, with a somewhat reduced performance due to a higher signal-to-noise ratio (Supplementary Fig. 24).

In summary, we here introduce a set of biodegradable, resilient materials for soft robotics, e-skins and healthcare that are healable, deformable, self-adhering and resistant to dehydration. We applied our materials approach to create a new set of durable biodegradable soft actuators and autonomous electronic platforms with multimodal sensing capabilities. Possible applications range from edible robotics, produce harvesting or animal behaviour studies to single-use scenarios in hazardous environments or medical settings, in which tools and healthcare devices are commonly disposed of after their employment to fulfil hygiene requirements. Implantable electronics or robots that operate underwater for an extended period of time still require biodegradable coatings that are hydrophobic, soft and at the same time stretchable. Our approach represents a frugal, environmentally benign and inexpensive route for future biodegradable technologies that avoid the incurrence of microplastics and are inherently safe when interacting with other lifeforms.

Online content

Any methods, additional references, Nature Research reporting summaries, source data, extended data, supplementary information, acknowledgements, peer review information; details of author contributions and competing interests; and statements of data and code availability are available at https://doi.org/10.1038/s41563-020-0699-3.

Received: 11 November 2019; Accepted: 6 May 2020;
Published online: 15 June 2020

References

1. Hoornweg, D., Bhada-Tata, P. & Kennedy, C. Environment: waste production must peak this century. *Nature* **502**, 615–617 (2013).
2. Leung, A., Luksemburg, W., Wong, A. & Wong, M. Spatial distribution of polybrominated diphenyl ethers and polychlorinated dibenzo-*p*-dioxins and dibenzofurans in soil and combusted residue at Guiyu, an electronic waste recycling site in southeast China. *Environ. Sci. Technol.* **41**, 2730–2737 (2007).
3. Baumgartner, M. et al. in *Green Materials for Electronics* (eds Irimia-Vladu, M., Glowacki, E. D., Sariciftci, N. S. & Bauer, S.) 1–53 (Wiley, 2017)
4. Irimia-Vladu, M. et al. Biocompatible and biodegradable materials for organic field-effect transistors. *Adv. Funct. Mater.* **20**, 4069–4076 (2010).
5. Boutry, C. et al. A stretchable and biodegradable strain and pressure sensor for orthopaedic application. *Nat. Electron.* **1**, 314–321 (2018).
6. Walker, S. et al. Using an environmentally benign and degradable elastomer in soft robotics. *Int. J. Intell. Robotics Appl.* **1**, 124–142 (2017).
7. Hwang, S. et al. A physically transient form of silicon electronics. *Science* **337**, 1640–1644 (2012).
8. Yang, C. & Suo, Z. Hydrogel ionotronics. *Nat. Rev. Mater.* **3**, 125–142 (2018).
9. Acome, E. et al. Hydraulically amplified self-healing electrostatic actuators with muscle-like performance. *Science* **359**, 61–65 (2018).
10. Someya, T. & Amagai, M. Toward a new generation of smart skins. *Nat. Biotechnol.* **37**, 382–388 (2019).
11. Li, C. H. et al. A highly stretchable autonomous self-healing elastomer. *Nat. Chem.* **6**, 618–624 (2016).
12. Cao, Y. et al. Self-healing electronic skins for aquatic environments. *Nat. Electron.* **2**, 75–82 (2019).
13. Wang, S. et al. Skin electronics from scalable fabrication of an intrinsically stretchable transistor array. *Nature* **555**, 83–88 (2018).
14. Wirthl, D. et al. Instant tough bonding of hydrogels for soft machines and electronics. *Sci. Adv.* **3**, e1700053 (2017).
15. Wang, X. et al. Food-materials-based edible supercapacitors. *Adv. Mater. Technol.* **1**, 1600059 (2016).
16. Bauer, S. & Kaltenbrunner, M. Built to disappear. *ACS Nano* **8**, 5380–5382 (2014).
17. Yang, J., Webb, A. R. & Ameer, G. A. Novel citric acid-based biodegradable elastomers for tissue engineering. *Adv. Mater.* **16**, 511–516 (2004).
18. Webb, A. R., Yang, J. & Ameer, G. A. Biodegradable polyester elastomers in tissue engineering. *Expert Opin. Biol. Ther.* **4**, 801–812 (2004).
19. Wang, Y., Ameer, G. A., Sheppard, B. J. & Langer, R. A tough biodegradable elastomer. *Nat. Biotechnol.* **20**, 602–606 (2002).
20. Cohn, D. & Salomon, A. H. Designing biodegradable multiblock PCL/PLA thermoplastic elastomers. *Biomaterials* **26**, 2297–2305 (2005).

21. Skarja, G. A. & Woodhouse, K. A. In vitro degradation and erosion of degradable, segmented polyurethanes containing an amino acid-based chain extender. *J. Biomater. Sci. Polym. Ed.* **12**, 851–873 (2001).
22. Averous, L., Moro, L., Dole, P. & Fringant, C. Properties of thermoplastic blends: starch–polycaprolactone. *Polymer* **41**, 4157–4167 (2000).
23. Zhu, C. et al. Highly stretchable HA/SA hydrogels for tissue engineering. *J. Biomater. Sci. Polym. Ed.* **29**, 543–561 (2018).
24. Shintake, J., Sonar, H., Piskarev, E., Paik, J. & Floreano, D. Soft pneumatic gelatin actuator for edible robotics. In *2017 IEEE/RSJ International Conference on Intelligent Robots and Systems (IROS)* 6221–6226 (IEEE, 2017).
25. Van Den Bulcke, A. I. et al. Structural and rheological properties of methacrylamide modified gelatin hydrogels. *Biomacromolecules* **1**, 31–38 (2000).
26. Wu, T. et al. A pH-responsive biodegradable high-strength hydrogel as potential gastric resident filler. *Macromol. Mater. Eng.* **303**, 1800290 (2018).
27. Ceseracciu, L., Heredia-Guerrero, J. A., Dante, S., Athanassiou, A. & Bayer, I. S. Robust and biodegradable elastomers based on corn starch and polydimethylsiloxane (PDMS). *ACS Appl. Mater. Interfaces* **7**, 3742–3753 (2015).
28. He, Q., Huang, Y. & Wang, S. Hofmeister effect-assisted one step fabrication of ductile and strong gelatin hydrogels. *Adv. Funct. Mater.* **28**, 1705069 (2018).
29. Qin, Z. et al. Freezing-tolerant supramolecular organohydrogel with high toughness, thermoplasticity, and healable and adhesive properties. *ACS Appl. Mater. Interfaces* **11**, 21184–21193 (2019).
30. Schrieber, R. & Gareis, H. *Gelatine Handbook* (Wiley, 2007).
31. Luo, Z. et al. Biodegradable gelatin methacryloyl microneedles for transdermal drug delivery. *Adv. Healthcare Mater.* **8**, 1801054 (2018).
32. Echave, M. et al. Enzymatic crosslinked gelatin 3D scaffolds for bone tissue engineering. *Int. J. Pharm.* **562**, 151–161 (2019).
33. Mandrycky, C. et al. 3D bioprinting for engineering complex tissues. *Biotechnol. Adv.* **34**, 422–434 (2016).
34. Kim, D., Lee, H., Kwon, S., Choi, H. & Park, S. Magnetic nano-particles retrievable biodegradable hydrogel microrobot. *Sens. Actuators B* **289**, 65–77 (2019).
35. Chambers, L., Winfield, J., Ieropoulos, I. & Rossiter, J. Biodegradable and edible gelatine actuators for use as artificial muscles. In *Proc. SPIE 9056, Electroactive Polymer Actuators and Devices* 90560B (SPIE, 2014).
36. Sardesai, A. et al. Design and characterization of edible soft robotic candy actuators. *MRS Adv.* **3**, 3003–3009 (2018).
37. Deng, Y., Zhang, Y., Lemos, B. & Ren, H. Tissue accumulation of microplastics in mice and biomarker responses suggest widespread health risks of exposure. *Sci. Rep.* **7**, 46687 (2017).
38. Feig, V., Tran, H. & Bao, Z. Biodegradable polymeric materials in degradable electronic devices. *ACS Centr. Sci.* **4**, 337–348 (2018).
39. Shimizu, S. & Matubayasi, N. Gelation: the role of sugars and polyols on gelatin and agarose. *J. Phys. Chem. B* **118**, 13210–13216 (2014).
40. Polygerinos, P. et al. Soft robotics: review of fluid-driven intrinsically soft devices; manufacturing, sensing, control, and applications in human–robot interaction. *Adv. Engin. Mater.* **19**, 1700016 (2017).
41. Amjadi, M., Kyung, K.-U., Park, I. & Sitti, M. Stretchable, skin-mountable, and wearable strain sensors and their potential applications: a review. *Adv. Funct. Mater.* **26**, 1678–1698 (2016).
42. Krause, J., Winfield, A. & Deneubourg, J. Interactive robots in experimental biology. *Trends Ecol. Evol.* **26**, 369–375 (2011).
43. Bogue, R. Fruit picking robots: has their time come?. *Ind. Robot* **47**, 141–145 (2010).
44. Hohimer, C. J. et al. Design and field evaluation of a robotic apple harvesting system with a 3D-printed soft-robotic end-effector. *Trans. ASABE* **62**, 405–415 (2019).
45. Hartmann, F., Drack, M. & Kaltenbrunner, M. Meant to merge: fabrication of stretchy electronics for robotics. *Sci. Robotics* **3**, eaat9091 (2018).

Methods

Materials. All chemicals were used as received without further purification. Gelatin powder (Bloom Factor 260, Ewald-Gelatine GmbH) was used for the main gel network, the sugar syrup contained 17% dextrose, 13.5% maltose, 12% maltotriose and 57.5% oligo/polysaccharides (Glucose Syrup 45°, Grafschafter Krautfabrik Josef Schmitz KG) as co-solvent, citric acid (Carl Roth GmbH & Co. KG) to adjust the pH value and glycerol (Rotipuran ≥ 99.5%, Carl Roth GmbH & Co. KG) to increase the bound-water content of the biogel. E471 (mono- and diglycerides of fatty acids) powder (Breinbauer Rohstoffe) was used as a stabilizer for the biogel foams and riboflavin (E101, R9504-25G, Sigma-Aldrich) was used for fluorescent biogels. Pure *Aloe vera* plant extract (local pharmacy) was used as an additive for a wound-healing biogel. We coloured biogels with food dyes (Online-Konditor Mark Bünger) for visualization. A composite of carnauba wax (local pharmacy) and graphite powder (Graphitan 7525, Ciba Specialty Chemicals Inc.) served as a temperature sensitive resistor. Zinc-foil sheets (50-µm thick, ZN000230, GoodFellow GmbH) served as the base conductive material for the sensor skins. Dewaxed Schellac (A. F. Suter & Co. Ltd) mixed with polyethylene glycol (PEG 400, Sigma-Aldrich) was used as an isolation layer for parts of the stretchable conductors of the pressure-sensor matrix (close to the connections to the logic board). Actuator casting moulds were printed using an acrylonitrile butadiene styrol filament and covered by a releasing agent that consisted of carnauba wax (local pharmacy), beeswax (local pharmacy), olive oil (local grocery store) and lecithin dissolved in water (E322, Breinbauer Rohstoffe).

Biogel preparation. Citric acid (1 g) and glycerol (8 g) were dissolved in deionized water (8 g) and heated to 60 °C. Sugar syrup (7 g) was heated to 60 °C to reduce its viscosity and mixed to the presolution. After cooling to room temperature, gelatin powder (4 g) was added and allowed to soak for 1 h. The mixture was heated in an oven at 70 °C for 1 h and stirred in a planetary mixer (DAC 600.2 VAC-P, Hauschild Engineering) under vacuum (2,350 r.p.m., 450 mbar) for 4 min to achieve a homogeneous precursor ready for moulding. Gel recipes with varying compositions used here are listed in Supplementary Table 3.

Biogel foam. E471 powder was dissolved in deionized water (ratio 1:2) for 2 h under vigorous stirring. The dissolved E471 (8 g) was mixed with the biogel presolution and gelatin powder (4 g) and allowed to soak for 1 h. The mixture was heated at 65 °C for 1.5 h and mixed with a hand blender for 30 s at 5,000 r.p.m., which resulted in a microfoam, which was cast into acrylic glass moulds.

Biogel thin films. The prepared warm liquid biogel was poured on a Teflon plate and distributed via doctor blading. The films were left to dry for 1 h, which resulted in a thickness of 0.58 mm. Coating with talcum powder rendered non-sticky films.

Biogels with biodegradable encapsulation. Shellac solution was prepared according to Luangtana et al.[46]. Schellac (36 g) was dissolved in ethanol (100 g). PEG 400 (7.2 g) was added to the shellac solution and stirred for 10 min. G2430 biogel samples were dip coated in the shellac solution four times, followed by 30 min of heating at 50 °C in an oven and a final heating at 70 °C for 1 min. We repeated this procedure to achieve a homogeneous encapsulation of thickness ~200 µm.

Degradation and ageing experiments. *BOD.* The ready biodegradability of gelatin biogels was investigated with closed bottle tests according to the Organisation for Economic Co-operation and Development guidelines for the testing of chemicals. The beginning and end of the biodegradation, and the aerobic decomposition of organic compounds were identified via the oxygen uptake. To perform the degradation, an aerated, tempered and inoculated mineral medium was prepared and stored sheltered from light. To investigate the oxygen uptake, test substances of the blank medium, a reference solution (medium + sodium acetate) and a test solution (medium + test sample) were prepared (300 ml). For the non-invasive analysis of the oxygen amount in the solutions, a phase fluorometer (Neofox-GT, Ocean Optics) and oxygen sensor patches (RedEye, Ocean Optics) were used. The BOD was calculated from the initial and actual mean amounts of dissolved oxygen in the solution (Supplementary Methods) and was measured in a daily interval until day 11 and in two-day intervals afterwards. All the measurements were performed in a dark and tempered (20 °C) room.

Mineral medium preparation. Four stock solutions were prepared (Supplementary Information) and 6 ml of each stock solution taken and diluted with 6 l of deionized water. To improve the preservability, six drops of concentrated hydrochloric acid were added. The mineral medium was stored for 24 h at 20 °C and subsequently inoculated with 0.3 ml of the secondary effluent of a sewage plant and aerated overnight.

Dehydration. Circular samples (20 mm in diameter) were punched out of 2-mm-thick gel sheets (G1620, G1636, G1644 and G1215f). The samples were placed on a needle-tip tripod to ensure air circulation on the entire sample surface and put on an analytical balance (AEJ 200–4CM, Kern & Sohn GmbH) in a climate chamber (20 °C, 40% RH). Additional drying experiments at a very low humidity (23 °C, 20% RH) were performed with the most drying-resistant gel (G1644; Supplementary Fig. 7). The RH and temperature inside the chamber and the weight of the gel sample were measured and logged once every minute.

Dissolution of biogels. Circular samples (20 mm in diameter) were punched out of 2-mm-thick gel sheets (G1620 and G1215f) and placed in a beaker filled with deionized water. The dissolution at constant temperature of 23 °C was captured with a camera (Fig. 1c and Supplementary Videos 1 and 2). Biogels with encapsulation were prepared as described above and equally tested in deionized water and citric acid solutions (pH 2.1), and trisaminomethane buffer solutions (pH 8.1) (Supplementary Video 3).

Influence of biogels on microbial growth. Sterile cell culture dishes were filled with autoclaved agar. Bacterial cells (XL1-Blue Competent Cells, Stratagene) were grown overnight in autoclaved lysogeny broth (Sigma-Aldrich). The overnight cultures (100 and 500 µl) were plated on agar plates. Gelatin samples (41.0 ± 8.0 mg) were placed on agar plates arranged in a circle. As a positive control, a circular piece of paper was soaked with 10× antibiotic/antimycotic (Sigma-Aldrich). The plates were incubated at 37 °C for 24 h. The growth of the bacteria was analysed visually and recorded using a digital camera.

Mechanical characterization of biogels. We used 2-mm-thick biogels for characterization. Standardized dumbbell-shaped samples (ISO527–2:1996(5A)) were punched out of biogel sheets for uniaxial tensile tests. All the biogels were unpacked from their moulds one week after casting. All the tests were performed in ambient air at room temperature if not mentioned otherwise.

Biaxial stretching and pressure–volume measurements. Squared biogel sheets (G1620, G2420 and G2820 of side length 40 mm) were coloured, mounted on a pressure vessel with a circular clamp (aperture 30 mm) and inflated with air until material failure. The volume of the inflated gel was calculated from its curvature obtained by video analysis. The pressure was measured with a sensor (JUMO dTrans-p30, Fulda).

Uniaxial tensile tests. Uniaxial tensile tests of biogels were performed with a custom-made tensiometer (stretching speed of 1.25 mm s^{-1}) inside a climate chamber (C-40/350, CTS Clima Temperatur Systeme GmbH) at constant climatic conditions (23 °C, 40% RH). The applied force was measured with a force gauge (KM26z 100N, ME-Meßsysteme GmbH), and the elongation was read from the step-motor controller (TMCM-1111, Trinamic). Single E values were calculated from a regression using the neo-Hookian model for incompressible elastomers. Samples with a varying amount of gelatin but unchanged quantity of all the other constituents were tested (samples G(09–28)20). The influence of the glycerol concentration was tested by changing the ratio of water and glycerol whereby the total amount of water and glycerol was kept constant at 52 wt% (samples G16(20–44)). To test the influence of storage time, biogels (G1620 and G1636) were stored under ambient conditions. Cyclic tensile tests of biogels (G1620 and G1215f) were performed by stretching to 100% ε_u for five cycles. The dissipated energy was calculated from the area between the extension and relaxation curves.

Peel tests. We measured the debond energy between the G1644 biogel (120 × 30 × 1.5 mm) and diverse substrates (PDMS, Ecoflex, porcine skin, paper, aluminium; 35 × 75 mm) via a 90° peel test. The biogel was covered with a 6-µm-thick polyethylene terephthalate (PET) foil after casting to prevent he elongation of the biogel during peeling. The porcine skin was pretreated by shaving and heating to 37 °C to mimic body temperature.

Fabrication of the biogel actuators. *Casting.* Biogel (G2430) precursors were moulded in 3D-printed preheated moulds in a two-step casting process. First, we cast a semi-open tube that was removed from its mould after cooling. Second, we cast a thin layer (a few millimetres) of precursor into the mould in which we inserted a silicone tube (outer diameter, 1.65 mm; inner diameter, 0.76 mm, Freudenberg Medical) and immediately inserted the semi-open tube into the precursor to close it (Supplementary Fig. 12).

Textile exoskeleton. The textile exoskeleton was crocheted with cotton yarn and designed to guide the motion of the biogel actuator. We fabricated two designs that enabled u-shaped and s-shaped motions, respectively. Both designs were based on a building block that consisted of interconnected ribs that allow for the deformation of the actuator tube and tightly connected meshes, which constrain deformation.

Actuator assembly. The biogel actuator tube was inserted into the textile exoskeleton and the ribs aligned in parallel. The rear end of the exoskeleton was sewed onto a connection plate to fix the actuator in different set-ups. The elephant head was assembled from laser-cut plywood plates.

Fluorescent actuator and elephant. The actuator tube and elephants were cast from a G2430r ultraviolet-fluorescent biogel and inserted into the s-shape exoskeleton. The actuator was inflated manually under ultraviolet illumination (365 nm, 120 m W cm^{-2}, LED-Spot 100 with a LED Powerdrive 40, Dr Hönle AG).

Actuator characterization. If not mentioned otherwise, all the tests were performed on a u-shaped actuator from the G2430 biogel under ambient conditions. The actuation stroke as a measure of actuator performance was measured with a force cell (KM26z 100N, ME-Meßsysteme GmbH).

Pressure control unit. The pneumatics included a compressor (N86KN.18, KNF Neuberger SAS) connected to a regulating valve, a solenoid valve (VDW Series, SMC) and the actuator. A second solenoid valve served as an air outlet for the actuator. A microcontroller (Arduino UNO, Arduino s.r.l.) operated the solenoid valves. The pressure was recorded using a pressure sensor (40PC Series, Honeywell).

Bending angle. To test the bending angle, the actuator was fixed in a vertical position and inflated using the pressure control unit until a full turn was achieved (Fig. 3e and Supplementary Fig. 18a).

Actuator simulation. We modelled the deformation field using the commercial FEM software ABAQUS/Standard (SIMULIA, Dassault Systemes) with a simplified model of the actuator.

Maximum force test. The actuator (133 mm in length) was put into a polyvinyl chloride tube (inner diameter, 27 mm; length, 90 mm) to keep the tip positioned perpendicular to the force cell (Supplementary Fig. 17). This constraint minimized the non-linear effects and kept the force concentrated on the tip. The pressure was controlled manually.

Durability test. The u-shaped actuator tubes were cast from the G2420 and G2430 biogels and fixed to the force cell in a perpendicular position. We repeatedly inflated the actuators with a constant pressure supply until the actuators either failed or the performance dropped to ~40%. Testing was performed inside the climate chamber at constant conditions (23 °C, 40% RH). To test the cyclic actuation with a constant force setting, we repeatedly inflated a u-shaped actuator made from the G2430 biogel until a force threshold of 0.2 N was reached. The base pressure was adjusted manually, if needed.

Stepwise actuation. We used the s-shaped actuator on the wooden elephant head for stepwise actuation. The pressure in the actuator was controlled by the maximum pressure and the inflation time. The inflation time was controlled by a microcontroller, which switched the solenoid valves. One complete inflation and deflation ramp started with the opening of the inflation valve for 1 s, followed by closing for 3 s (hold time) and then opened again for another second with a 3 s hold time. For deflation, the deflation valve was opened for 1 s with a 3 s hold time and again opened for 4 s. Then the program was started again with the inflation steps.

Suction cup fabrication and lifting of objects. For the suction cup, we printed a two-part mould with a silicone tube (outer diameter, 1.65 mm; inner diameter, 0.76 mm, Freudenberg Medical) inserted at its bottom and cast the suction cup from a G2430 biogel. A vacuum was applied manually with a syringe.

Pressure sensor. *Assembly.* Biogel foam sheets (G1215f, 2 mm in thickness) were cast and dried in ambient conditions for one week to reduce the thickness to ~1.2 mm. Disks (12 mm in diameter) were punched out and circular zinc-foil electrodes (10 mm in diameter) were attached on both sides.

Characterization. The pressure sensor was mounted on a rigid plate in a compression tester (2.5-kN load cell, Zwick Roell Z005) and pressed by a cylindrical indenter (10 mm in diameter). We measured the impedance change using an impedance analyser (1 kHz, 1 V, 4284A Precision LCR Meter, HP).

SEM. Thin strips of G1215f biogel foam were prepared and 10–15 nm of gold (99.99% Au, Oegussa) were thermally evaporated (0.1–0.3 nm s^{-1}, 1×10^{-6} mbar) for an improved surface conductivity. The measurement was performed using a Zeiss 1540 XB CrossBeam SEM with an acceleration voltage of 3 keV.

Pressure sensor on the actuator. Circular zinc electrodes (2 mm in diameter) were attached on both sides of a biogel foam disk (4 mm in diameter). The pressure sensor was mounted on a u-shaped actuator using gold wires. We actuated the sensor-equipped actuator against the thorn of a rose or against a screwdriver and measured the signal change of the deforming sensor. Reaching a certain threshold immediately triggered a relaxation of the actuator.

Read-out of the pressure sensor on the actuator. The pressure sensor was connected to a function generator that provided a sine wave with a 1 V amplitude, 2 kHz and 2.5 V offset. We included the pressure sensor in a voltage-divider circuit to measure the voltage drop due to a capacity change of the sensor.

Toy robot. We crocheted 'Percy the Gellyfant' from a pattern designed by M. May (Mostly Stitchin' Crochet). We used our textile exoskeleton design for the trunk, together with a smaller actuator tube, connected to a silicone tube. The trunk was actuated manually using a syringe.

LARH and rapid assembly. *LARH.* Biogel samples (2 mm in thickness) were cut with a knife and placed with a cleavage of less than 1 mm. The area around the cut interfaces was irradiated with a CO_2 laser (Speedy300, Trotec Laser GmbH) (10.6 µm) in engraving mode, which caused the biogel to melt locally and heal. The engraving pattern was repeated five times to ensure a full healing of the samples.

Tensile tests. Half of the dumbbell-shaped samples (G1620) were cut in the centre perpendicular to the stretching direction and healed by the LARH method. Uniaxial tensile tests were performed on both the pristine and healed samples.

Trefoil knot. Rectangular strips of G3030, G2430 and G1730 biogels (5 × 30 mm) were cut from 2-mm-thick sheets and coloured green, blue, and orange respectively. The strips were assembled in series, healed with the LARH method, arranged in the trefoil knot configuration and healed again at the open ends.

Graded modulus gels. Rectangular strips of G3030 (25 × 20 mm), G2430 (15 × 20 mm) and G1730 (25 × 20 mm) biogels were cut from 2-mm-thick sheets and coloured green, blue and orange, respectively. The strips were assembled in series and healed with the LARH method. They were then mounted in a uniaxial stretching device with 10-mm-broad clamps to leave three unconstrained segments of length 15–17 mm each. The sample was manually stretched to a maximum total strain of 50%. We calculated the overall strain behaviour analytically by linearizing the stress–strain relationship and applying rules for the composite materials. FEM modelling of the deformation field was performed by simplifying the material behaviour with the neo-Hookean model.

Biodegradable sensors and hybrid e-skins. *Sensor fabrication.* The biodegradable sensors and conductors were fabricated on biogel strips by structuring the applied zinc foil with a laser cutter and removing excess material. Stretchable conductors and humidity sensors were fabricated on the G2430 biogel, strain sensors on the G1730 biogel and temperature sensors on the G3030 biogel. For the temperature sensor, temperature-sensitive wax at 80 °C was coated through a mask (5 × 3.4 mm) on the centre of the sensor.

Sensor characterization. All the sensors were characterized inside the climate chamber. Resistance changes of the conductors and temperature sensors were recorded with a multimeter (Keithley Model 2000). Impedance changes of the strain and humidity sensors were recorded with an impedance analyser (1 kHz, 1 V, 4284A Precision LCR Meter, HP). Uniaxial cyclic tensile tests were performed at 23 °C and 40% RH.

Flexible PCB and control units. The flexible PCB hosting all the control, power and communication electronics was designed and routed inhouse and externally fabricated (50 µm of polyimide coated with 18 µm of copper on the top and bottom layers). All the components were soldered onto the flexible PCB with standard solder (Sn60Pb39Cu1, RS Components).

Sensor-patch assembly. Strips of G3030 (green), G2430 (blue) and G1730 (orange) biogels were arranged and healed with the LARH method to form a patch with a graded E (Extended Data Fig. 3). Zinc foil was placed on the patch and structured with a laser cutter. After peeling off the excess material, temperature-sensitive wax was coated onto the patch through a mask (5 × 7.5 mm and 5 × 4 mm) and the flexible PCB was soldered to the contacts of the e-skin.

Sensor-patch characterization. The sensor patch was placed in the climate chamber and connected to a computer via the low-energy Bluetooth module. Climatic conditions were varied from 20 to 30 °C in temperature and from 40 to 60% RH in humidity. The impedance ($|Z|$) of each sensor was logged at a frequency of 10 kHz for 1 min in each climatic configuration, which gave the sensor characteristics.

On-skin tests. The arms and/or hands shown in Fig. 4, Extended Data Fig. 6 and Supplementary Video 10 are those of M.B., who gave her permission to publish in these media. We measured the temperature change of the e-skin in proximity to a cup filled with boiled water, the impedance changes due to a humidity change through aspiration and the strain response due to deformation. The data were wirelessly transmitted to a computer via the Bluetooth module.

In a second test, the biogel adhesion to human skin was tested. Two samples of the G1730 biogel of thicknesses 1 and 2 mm and a diameter of 2 cm were prepared. To enhance the adhesion, the biogel discs were moisturized before they were applied on the skin of the upper arm. The top side of the discs was covered with talcum powder to prevent sticking to the surrounding. The test started at 09:00 with normal daily activities, which included a 30-min walk outside (25–30 °C, ~50% RH). The participant ran for 60 min (13:00 to 14:00) to show the adhesion during sports activities. Additionally, the participant exercised with dumbbells to increase the arm movement. The biogel was removed after 7 h (Extended Data Fig. 6e,f).

In a third test, rectangular strips (25 × 100 × 2 mm) of the G1730 biogel were attached to the skin, as described above. The samples were worn for on the skin for 9, 16, 28 and 38 h (5–12 h each day) during normal daily activities.

Dumbbell-shaped samples were punched out of the strips and characterized with tensile tests. The resulting mechanical properties were compared with reference samples of the same batches stored at ambient conditions for the same time.

Touch sensor array. A sheet of biogel foam (G1215f, 67×105×1 mm) was partially coated with shellac to reduce the cross-talk between stretchable conductors. Zinc foil was structured with the laser cutter and gently pressed onto the foam under heat to leave a 4×4 touch sensor array. The flexible PCB was soldered to the stretchable conductors. Touch signals were read out at 80 Hz by impedance converters and wirelessly transmitted. We put cylindrical weights of 10, 20 and 50 g of diameters 12, 15 and 20 mm, respectively, onto a single sensor to test its performance. We successively put a 20-g weight onto four sensors of the array to test the signal responses of sensors. We placed a frame (inner side edge, 21 mm; outer side edge, 38 mm) onto the touch sensor array, together with a 500 g weight as an example for object detection.

Data availability

All the data needed to evaluate the conclusions in the paper are present in the paper and/or the Supplementary Information. All source files and experimental data are freely and publicly available at www.gel-sys.eu. Additional data related to this paper may be requested from the authors.

References

46. Luangtana-anan, M., Nunthanid, J. & Limmatvapirat, S. Effect of molecular weight and concentration of polyethylene glycol on physicochemical properties and stability of shellac film. *J. Agric. Food Chem.* **58**, 12934–12940 (2010).

Acknowledgements

This work was supported by the European Research Council Starting Grant 'GEL-SYS' under grant agreement no. 757931, the Austrian Research Promotion Agency GmbH (FFG) within the COMET-project TextileUX under grant agreement no. 865791 and through start-up funding of the Linz Institute of Technology (LIT) 'Soft Electronics Laboratory' under grant no. LIT013144001SEL. M.B. received support from Borealis and the Borealis Social Scholarship, VDI and the Dr Maria Schaumayer Foundation. G.B. acknowledges financial support from the European Commission within the 'LiNaBioFluid' project within the scope of H2020-FETOPEN-2014-2015-RIA. We thank Ewald-Gelatine, especially T. Hilt, for material support and fruitful discussions. We dedicate this work to S. Bauer.

Author contributions

M.B., S.B. and M.K. conceived the research project; M.B. developed the materials with input from G.B. and S.H.; F.H., M.B. and M.D. designed the experiments; M.B., L.L., D.P., F.H. and L.R. prepared the materials; F.H., M.B., D.W., L.R., L.L., F.G., M.S. and E.B. conducted the mechanical materials characterization; M.B., R.G. and D.P. performed the BOD and dissolution tests; S.D. recorded the SEM images; G.M. and F.H. conducted the mechanical simulations and modelling; M.B., D.P. and F.H. developed and characterized the soft actuator; F.H., R.P., M.D. and T.S. developed and characterized the degradable sensor patches; R.P. and D.S. developed the flex, PCB and software; S.K. performed the bacterial growth tests; F.H., D.W. and M.D. analysed the data; M.K. gave input at all the stages; F.H., M.B., M.D., D.W. and M.K. wrote the manuscript; all the authors contributed to editing the manuscript. M.K. supervised the research.

Competing interests

The authors declare no competing interests.

Additional information

Extended data is available for this paper at https://doi.org/10.1038/s41563-020-0699-3.

Supplementary information is available for this paper at https://doi.org/10.1038/s41563-020-0699-3.

Correspondence and requests for materials should be addressed to M.K.

Reprints and permissions information is available at www.nature.com/reprints.

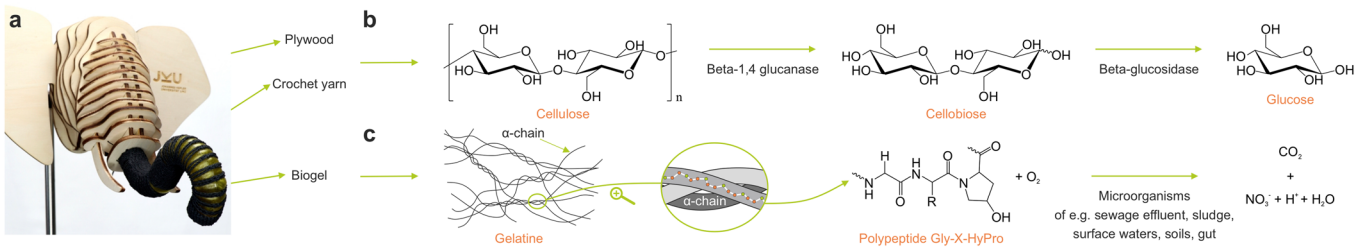

Extended Data Fig. 1 | Degradation of biomaterials. a, A bioinspired soft actuator consisting of wood, cotton-yarn, and gelatin-based biogel. **b**, Degradation reaction and end product of cellulose. **c**, Degradation and end product of gelatin. Single polypeptide strands are split by microorganisms found in waste water, gut, or soils.

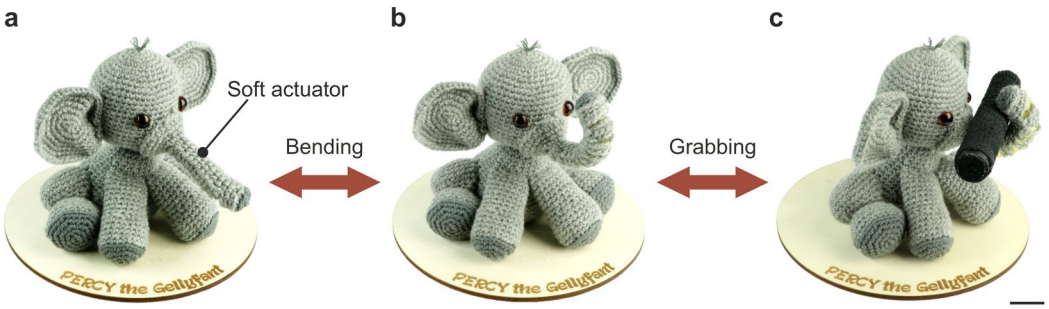

Extended Data Fig. 2 | Biodegradable soft robot demonstrator "Percy the Gellyfant". a, The manually actuated elephant trunk in its relaxed state and **b**, actuated u-shaped state. **c**, U-shaped movement allows grabbing of various objects. Scale bar, 2 cm.

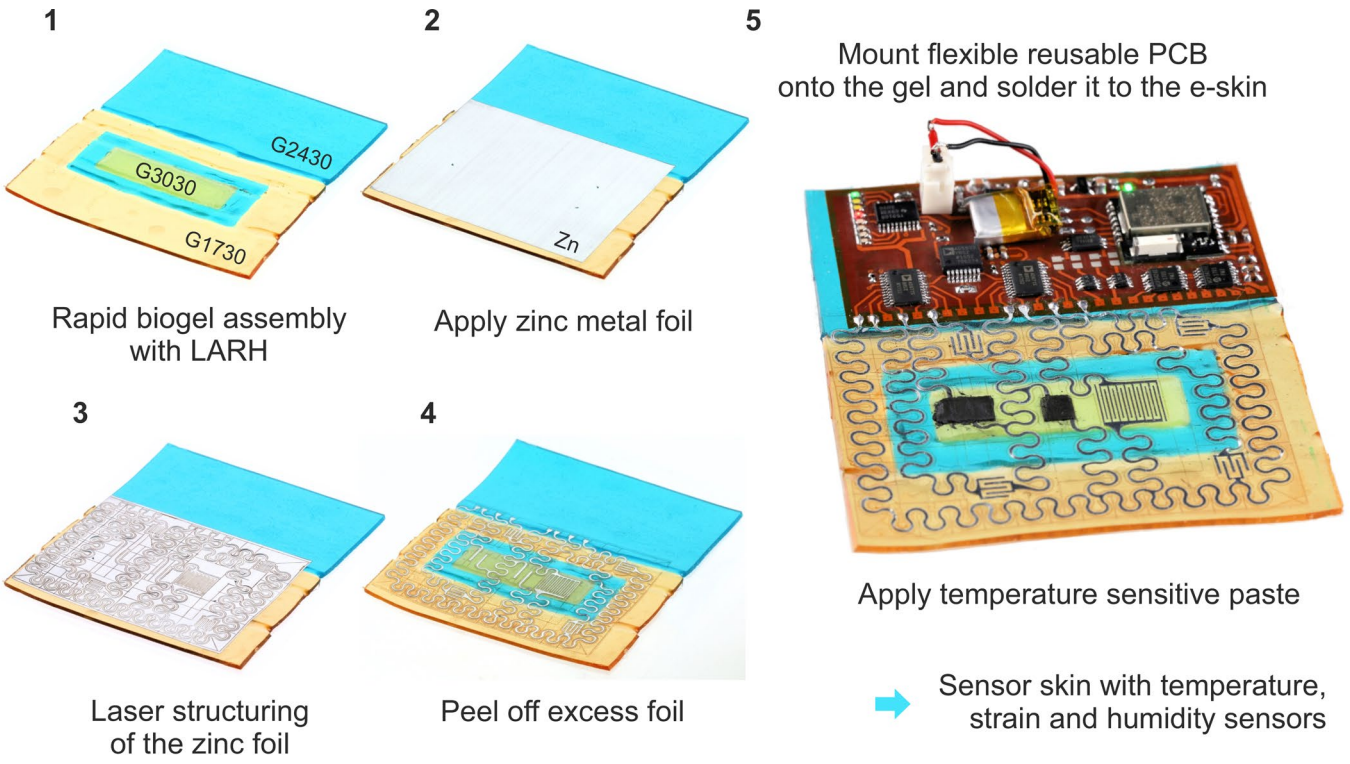

Extended Data Fig. 3 | Assembly of sensor skins. Assembly process of the sensor skin consisting of degradable e-skin and reusable PCB. **1**, Gels of different mechanical properties are joined by laser assisted rapid healing (LARH). **2–3**, A zinc metal sheet is then applied to the gel and structured by a fiber laser. **4**, After the structuring process the zinc residues are peeled off. **5**, A flexible reusable PCB is mounted on the gel and soldered to the zinc foil of the e-skin. In the last fabrication step a temperature sensitive paste is placed on the gel to finalize the temperature sensor.

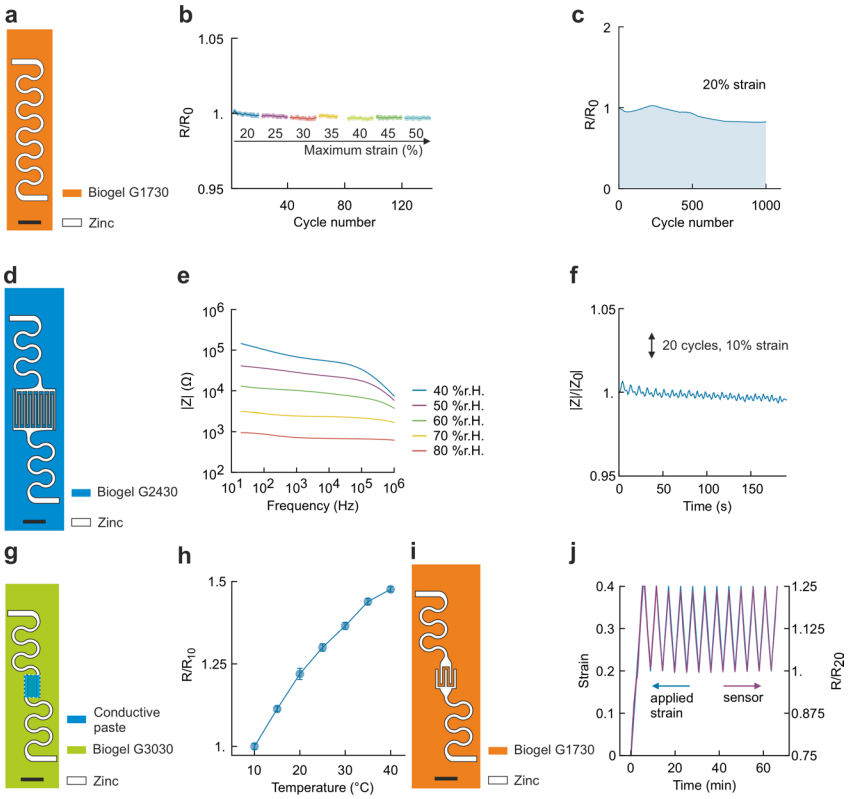

Extended Data Fig. 4 | Biodegradable sensors characterization. a, Stretchable meanders of zinc foil serve as conductors on biogels (G1730). **b**, Repeated stretching and increase of the maximum strain does not affect the conductivity of the zinc meanders. Mean resistance changes (solid line) during stretch-release cycles (data envelope) are shown. **c**, Those are durable for over 1000 stretching cycles, when stretched to a maximum strain of 20 %. **d**, Humidity sensors are realized with structured zinc foil on biogels (G2430). **e**, The magnitude of the impedance *Z* is measured as function of frequency at different climatic conditions, showing a change of two orders of magnitude. **f**, The sensor response is below 1 % when stretched repeatedly to a maximum strain of 10 %. **g**, Temperature sensors are realized with a conductive paste between two stretchable conductors on a biogel (G3030). **h**, The conductive pastes, fabricated on glass substrates, show a change larger than a factor of 2 over a range of 30 °C. Error bars, standard deviation for a measurement period >10 min. **i**, Strain sensors are designed with 5 fingers total to allow displacement of the electrodes. **j**, The sensor signals follow the applied strain profile linearly. Repeated cycles are tested between 20 % and 40 % strain, to account for irreversible mechanical deformation of the substrate during the first stretch-release cycle. Scale bars, 5 mm.

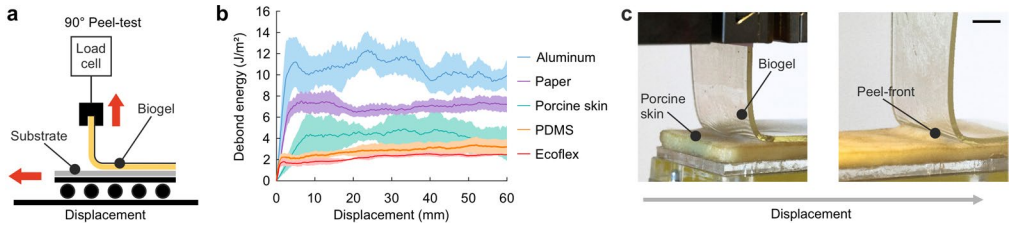

Extended Data Fig. 5 | Adhesion tests. a, Schematic of the 90° peel-test used to measure the debond energy between a biogel slightly pressed against diverse substrates. A 6 µm thick PET foil serves as stiff backing to prevent elongation of the peel arm, whereas a linear guiding ensures a constant angle of 90°. **b**, Measured debond energy for aluminum (blue), paper (purple), porcine skin (turquoise), PDMS (orange) and Ecoflex (red). **c**, Photographs of a biogel-porcine skin peel-sample taken during a peel-test showing the propagation of the peel-front between biogel and substrate. Mean values (solid line) and standard deviation (shadow) for $n > 4$ samples each. Scale bar, 1 cm.

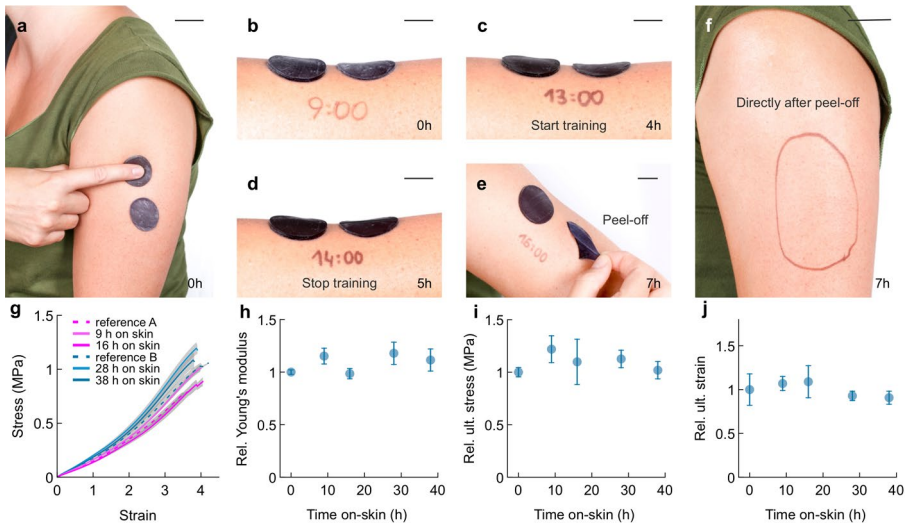

Extended Data Fig. 6 | On skin test – long time adherence. a, Two gel discs (G1730) with a thickness of 1 mm and 2 mm and a diameter of 2 cm were applied on the skin of the upper arm with little pressure. Scale bar, 2 cm. **b**, The test started at 9am, **c**, and showed no signs of gel disintegration during 4 h of wearing. Scale bars, 1 cm. **d**, Even after sports activities (13 pm to 14 pm) that involved higher mechanical load and sweating, there are no signs of detachment. Scale bar, 1 cm. **e**, After 7 h the biogel still adheres to the skin, even at the edges of the gel. Scale bar, 1 cm. **f**, The gel can be removed with no visible irritations after removal. Scale bar, 2 cm. **g**, Rectangular stripes were applied on the skin for up to 4 days (5–12 h each day) and compared to reference samples of the same batch. Mean values (solid line) and data envelope (gray shadow) for $n > 3$ samples each are shown. The biogel mechanics do not change upon wearing, even after 38 h wear-time on skin, resulting in constant **h**, Young's modulus (ref. A: 170 kPa ± 4 kPa, ref. B: 207 kPa ± 5 kPa), **i**, ultimate stress (ref. A: 830 kPa ± 60 kPa, ref. B: 1070 kPa ± 26 kPa), **j**, and ultimate strain (ref. A: 373 % ± 26 %, ref. B: 423 % ± 22 %). Error bars, standard deviation for a $n > 3$ measurements.

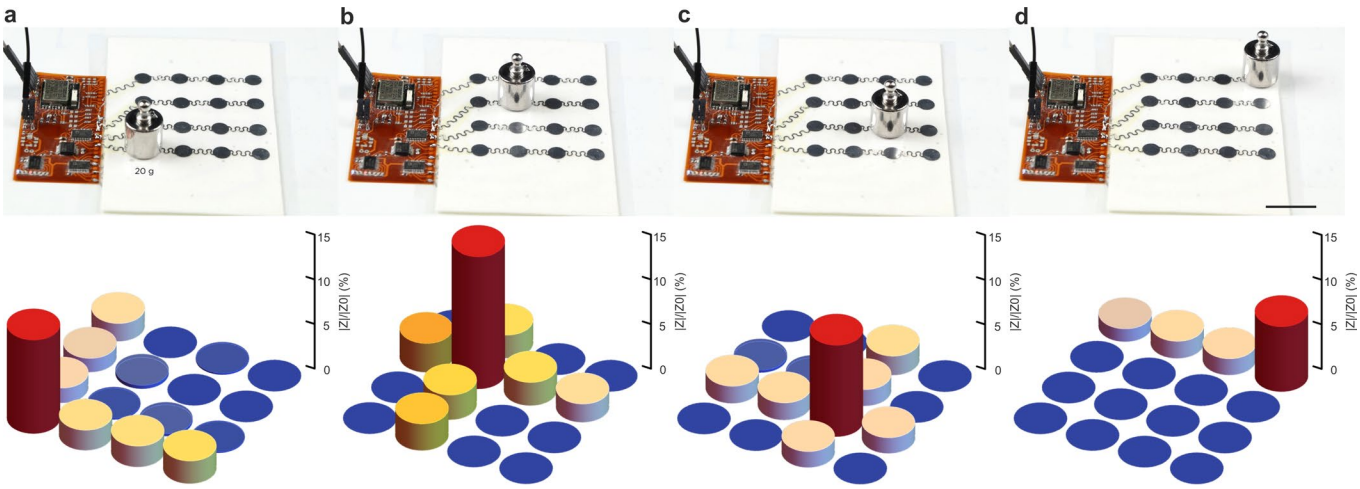

Extended Data Fig. 7 | Pressure skin. a–d, A weight of 20 g is applied to single pixels of the pressure skin sensor matrix. The measurement shows an impedance increase of 7–15 % compared to the initial value. Scale bar, 2 cm.